Estimating Nanoscale Deformation in Bone by X-ray Diffraction Imaging Method

Shigeru TADANO [1]*, Bijay GIRI [1], Takuya SATO [1], Kazuhiro FUJISAKI [2], Masahiro TODOH [1]

[1] Division of Human Mechanical Systems and Design, Graduate School of Engineering, Hokkaido University, Sapporo, Japan

[2] VCAD Research Program, Institute of Physical and Chemical Research (RIKEN), Wakko, Saitama, Japan

* Corresponding Author:
Shigeru TADANO, PhD
Professor, Division of Human Mechanical Systems and Design, Graduate School of Engineering, Hokkaido University
N13 W8, Kita-ku, Sapporo 060-8628, Japan
Tel/Fax: +81-11-7066405, E-mail: tadano@eng.hokudai.ac.jp

Keywords: Lattice strain, Cortical bone, X-ray diffraction, Imaging plate, Segmental-shift

Word count: 3562 words (Introduction through Concluding remarks)

Manuscript Type: Original Article

Abstract

Knowledge of internal stress-strain in bone tissue is important for clinical diagnosis and remedies. The inorganic mineral phase of apatite crystals in bone composite, because of its crystalline nature, provides a reliable way of measurement through X-ray diffraction system. Use of a two-dimensional detector, imaging plate, is considered to expedite the process with much more information, hence, is widely applied in the study of organization, stress, strain, etc for crystalline substance. The distortion of Debye rings in the image obtained by imaging plate can be directly related to the deformation in lattice plane of the crystals. Since X-ray diffraction method involves measurement at nano-level, proper focus on the extraction of data and corresponding analysis is needed. In the current work, we considered weighted average value of intensity to locate radius vectors along azimuthal direction in the diffracted rings from the primary array of digital data in steps of pixels. The widely applied approaches for profile shift measurement - peak-shift and full width at half maximum (FWHM) of a peak, and shift of centre of gravity of profile – were compared with a new concept of segmental-shift (SS) proposed previously by the authors. We observed reliable and effective outcomes with higher precision in the consideration of SS while using imaging plate as a detector. Our approach in this work for intensity integration and radius vector positioning especially add precision in such applications.

1. Introduction

Bone, a complex tissue with hierarchical structure in different structural levels, has provided challenging opportunities for researchers to reveal its complexity with numerous approaches from a macro-level to nano-level. At nanoscale range, the existence of apatite minerals (close to hydroxyapatite) embedded in collagen matrix is basically considered for nanostructure level study because of crystalline nature. The toughness of bone is believed to be influenced by the collagen matrix and stiffness by apatite crystals (Currey, 1969). Hence, understanding the mechanical behavior of these crystals is very important to analyze the mechanical properties of bone properly.

Because of non-destructive and non-invasive advantages of X-rays and predictive diffraction patterns with crystals, it has been widely applied to reveal various aspects of crystalline materials and in very few approaches in the case of biological tissues like bone (Almer & Stock, 2005; Borsato & Sasaki, 1997; Fujisaki & Tadano, 2007; Giri *et al*, 2007; Gupta *et al*, 2006; Tadano & Okoshi, 2006). Some attempts on the use of X-rays in fibril level of bone also exist (Almer & Stock, 2007; Gupta *et al*, 2006, 2005, 2004). The spacing between different lattice planes at the molecular level (interplanar spacing) gets deformed from its original dimension because of stress. Such change can be observed and measured by the deformation in different crystalline planes of the crystals. Thus the precise measurement of strain at molecular level and its correlation to the macroscopic deformation of overall tissue is highly desired to reliably estimate stresses in bones.

X-rays, after penetrating a polycrystalline subject, are diffracted by a family of crystallographic planes forming series of diffraction cones (Cullity & Stock, 2001). These cones appear as circular intensity rings in the transmitted diffracted beams, known as Debye rings, when detected in a two-dimensional detector placed normal to

it. Application of stress produces the change in interplanar *d*-spacing, which ultimately results in the distortion of these Debye rings in the detector. The amount of distortion according to the direction of applied stress gives the estimate of lattice strain (He and Smith, 1999). Such two-dimensional detector systems have advantages over conventional one-dimensional linear detector systems, since many orders of Bragg's reflection can be collected simultaneously and analysis could be done in wider aspect. In general, the procedure of extracting data from the two-dimensional detector for strain calculation consists of – (i) obtaining intensity distribution along a radial line of Debye rings, (ii) obtaining diffraction peaks by peak fitting routine, (iii) calculating displacement in the diffraction profile, and (iv) using the displacements to calculate strain. Imaging plate, a two-dimensional detector, can detect the diffracted Debye rings from different lattice planes simultaneously, and hence information along all the radial directions can be obtained from a single exposure. Because of this advantage, strain along any radial direction can be obtained by calculating deformation along any particular Debye ring.

In X-ray diffraction procedure of strain determination, generally one-dimensional diffraction profile is obtained either by scanning point detectors or linear position-sensitive detectors, or by using two-dimensional area detectors. The strain induced is then estimated by the shift in diffracted intensity profile from initial position to the position after being deformed. Hence the corresponding analyses and their accuracy or precision solely rely on the pattern of diffracted intensity obtained in the methodology used for respective approximation.

Most of the existing literatures on bone stress-strain analyses are found to consider widely applied peak-shift and full width at half maximum of a peak (FWHM) in a diffraction profile (Almer & Stock, 2005; Borsato & Sasaki, 1997; Gupta *et al*, 2006),

where the analysis is done using segment of profile. Among different standard peak determination techniques, shift of centre of gravity of profile is also used known as centroid method, which is useful during full profile consideration (Cullity and Stock, 2001; Noyan and Cohen, 1987). In peak-shift approach, simply the displacement of peak of the diffraction profile is considered, whereas in FWHM approach, shift of width of the profile at half of the peak-height is considered (Fig. 1a). In centroid-shift method (CS), shift of centre of gravity of the profile is calculated. Owing to different diffraction characteristics of mineral with broader profile, the authors (Fujisaki *et al*, 2006) proposed a new method by considering the integrated shifts in the segment (segmental-shift, SS) of diffraction profile to measure the change in lattice spacing of apatite crystals. According to this approach, every point ($2\theta_i^0$, I_i^0) of the non-strained profile shifts to a point ($2\theta_i^s$, I_i^s) on the strained profile related by Eq. (1) at constant strain, ε, defined as the point ($2\theta_i^c$, I_i^c) on the strained profile (Fig. 1b).

$$2\theta_i^c = 2\sin^{-1}\left\{\frac{\sin\left(2\theta_i^0/2\right)}{\varepsilon+1}\right\} \tag{1}$$

$$I_i^c = I_i^0 \quad \left(i = 1,2,3,\cdots,n\right) \tag{2}$$

The deviation of calculated values from the measured values, e_i was minimized to obtain the optimized strain (refer to Fujisaki *et al*, 2006 for detail). The authors applied similar approach in the lattice strain measurement of bone using a linear detector (scintillation counter) with improved accuracy compared to other approaches (Fujisaki and Tadano, 2007).

Compared to one-dimensional detector, the application of two-dimensional detector is very sensitive to the experimental condition, way of data extraction from the source, method applied in the analysis of data, and more. In the current work, we calculated strains in cortical strips of the bovine femur using widely accepted standard

approaches, *viz* peak shift, shift of FWHM and centroid-shift of diffraction profile and compared them with the segmental-shift method proposed by the authors (Fujisaki *et al*, 2006). From the comparative results, we attempted to address issues of accuracy and precision in strain measurements with the two-dimensional detector. We also considered a different approach, weighted average of intensities, for intensity integration and radial vector positioning from the array of two-dimensional pixel images raw digital data. Such critical issue of precision in locating a position in the diffraction profile is neither found to be focused nor discussed in related studies. Except these, we pointed out some of the overlooked issues that may affect the accuracy and precision while using two-dimensional detectors.

2. Materials and Methods

Specimen

The fresh femur sample was obtained from 24 months old female bovine donor. Mid cortical shaft of the femur was cut and frozen at -30^{o}C until further preparation.

Cortical strips of size 40×6×0.8 mm having osteonal and lamellar microstructure were harvested from the mid femoral shaft with the longer axis of the strips along the femoral axis. Rough cuts were done using hand-saw and finished cuts using the circular diamond blade saw. The surfaces of the specimens were gradually smoothed in series of emery papers and polished in diamond paste. The samples were washed in the ultrasonic bath with physiological saline during every step of grinding and polishing. Precaution was taken to avoid extra heating of the specimens during all the steps.

The strain gage was glued with Cyano-Acrylate base Strain Gage Cement (KYOWA, Japan) on the surface near to one of the ends of the specimen to record

applied strains (Fig. 2).

X-ray diffraction imaging system

Two-dimensional X-ray detector based on the imaging plate technology is popularly applied technology in X-ray diffraction procedures, since it incorporates advantages of both conventional X-rays photographic technique and linear detectors. The imaging plate technology consists of the X-ray storage phosphors plate called 'Imaging Plate (IP)', a reusable two dimensional X-ray recording film. Figure 3a shows the schematic representation of the laboratory X-ray diffraction imaging system. The experimental set up is shown in Fig. 3b. X-rays diffracted through the specimen are absorbed by the IP.

X-rays with characteristics Mo-Kα, Mo target, wave length 0.071 nm, tube voltage 40 kV and tube current 40 mA were generated from RINT2000 X-ray diffraction system (Rigaku Co., Japan). Collimator of diameter 1.0 mm was used to target the beam perpendicular to the specimen. IP (BAS-SR 127 mm × 127 mm, Fuji Photo Film Co. Ltd., Japan) was used to detect the transmitted radiation through the specimen. The specimen and the detector were placed parallel throughout the experiment. R-axis DS3C scanner (Rigaku Co., Japan) was used to readout X-ray data detected by the IP.

Experiment and Analysis

The specimen was mounted to the screw-driven tensile loading device developed in our laboratory keeping long axis of the specimen along the loading direction (Fig. 2). After 10 minutes exposure, the IP was readout using the scanner. A two-dimensional X-ray diffraction pattern was obtained in 1140×1140 pixels area image

(100 μm/pixel resolutions) (Fig. 4) by using a software compatible with the scanner. The beam centre was determined by allowing direct beam for a short duration in the absence of specimen. Using the calculated beam centre as the centre of Debye rings, the intensity pattern was converted to Cartesian distribution (diffraction angle '2θ' as abscissa and intensity values 'I' as ordinate) for every degree of azimuthal interval (β).

The pixel step being 100 μm in this case, actual radius vector position lying within one pixel square cannot be obtained accurately by direct pixel data. Here, we applied the weighted average of nearby pixel intensity values for each geometrically calculated radius vector position. For each calculated position, the nearby pixel intensities were divided by the distance from the calculated position and weighted average intensity was obtained. The distribution patterns were obtained for unstressed sample, sample stressed at 500, 1000, 1500 and 2000 micro-strains. The loading device was manually adjusted for constant strain readings in the digital strain indicator. The *(211)* diffraction profile was used for the analysis. Lattice strains at different azimuthal angles were calculated using the shift in peak position, shift in FWHM, shift in centroid and shift in whole profile segment (segmental-shift). Strains for each azimuthal direction were calculated according to Eq. (3), derived from Bragg's law ($2d \sin\theta = n\lambda$) (Fig. 3a).

$$\varepsilon_{hkl} = \frac{d - d_0}{d_0} = \frac{\sin\theta_0 - \sin\theta}{\sin\theta} = \frac{\sin\left[\frac{1}{2}\tan^{-1}\left(\frac{r_0}{L}\right)\right] - \sin\left[\frac{1}{2}\tan^{-1}\left(\frac{r}{L}\right)\right]}{\sin\left[\frac{1}{2}\tan^{-1}\left(\frac{r}{L}\right)\right]} \qquad (3)$$

Here, d is interplanar distance, θ is diffracted angle, r is radius vector of Debye ring, and L is camera length (140 mm in this case). The sub-script '*0*' indicates values at unstressed (initial) state.

The deformations at the irradiation area and strain gage location are assumed to be identical, since they lie along the same loading line.

3. Results

Figure 5 represents strain distribution of *(211)* plane along azimuthal directions, β (specimen, n = 3). The measured strain distribution (lattice strain, ε_h) at different sample strains (ε_b) were plotted using peak-shift, shift of FWHM, centroid-shift and segmental-shift approaches. Maximum strains were observed around loading direction, i.e. bone axis (near β = 90 degrees). Minimum strains were observed perpendicular to the loading direction (near β = 0 & 180 degrees). The distribution profiles are smoother at higher sample strain. The region above zero-strain line represents the tensile region, whereas the region below zero-strain line is the compression region. Figure 6 shows correlation between applied sample strain (ε_b) and lattice strain (ε_h) measured along the loading direction (specimen, n = 5). The strains are linearly correlated in all the cases. But the segmental-shift approach showed close relationship with highest R^2 value (99.49 %) compared to peak-shift (R^2 = 98.44 %), FWHM (R^2 = 95.24 %) and centroid-shift (97.76 %) approaches. The mean of measured strain (lattice strain, ε_h) to applied strain (tissue strain, ε_b) ratios were also plotted for all the cases (Fig. 7). The error bars represent standard deviation.

We also compared our previous results obtained by using scintillation counter (Fujisaki *et al*, 2006) with the current results from IP. Figure 8 represents mean of lattice strain (ε_h) along loading direction (specimen, n = 5) with error bar representing

standard deviation. With segmental-shift approach, lower deviation range was observed compared to peak-shift and FWHM approaches similar to previous results. Furthermore, the deviations in all the three approaches are found less while using imaging plate.

4. Discussion

The general measurement procedures for most of the imaging methods make use of digital data in pixels. It is advantageous using imaging plate as a detector since lot of information can be extracted within a short interval of time. The wide application of this technology is basically in stress and strain analysis of crystalline materials, where the shift in intensity peaks along particular direction after loading is considered. In the application of imaging plate as a detector, the scanned digital data contains intensity values in terms of the pixel coordinates of the detector image. Different facilitating software and programs are available for extracting information of interest from the diffraction data (Hammersley *et al*, 1996; Rodriguez-Navarro, 2006), but in all the cases step size of intensity values is limited by the number of pixels in the image. According to resolutions preferred during scans (e.g. 50 μm/pixel, 100 μm/pixel, etc), the pixel step size varies and hence the position of peak may differ. On the other hand, increasing number of pixels (decreasing step size) will result lengthened period of data processing. The distribution of intensity (or peak position) also differs depending on intensity density gathered from imaging plate readout, which depends on the duration of X-rays exposure as well as the surface finish of diffracting samples. Furthermore, the approximations used for peak fitting and thereby associated considerations like peak position, FWHM, total integrated intensity, centre of gravity, etc of diffraction profile will also have effect on the final result,

especially for peak broadened profile. To resolve this to some extent, the authors proposed a new method for the diffraction profile shifts using a linear detector, scintillation counter (Fujisaki *et al*, 2006). In this regard, to explore the difficulties of precision in such applications, we attempted to provide some comparative outcomes involving the standard approaches as well as tried to address the ignored consideration on intensity integration and radius vector positioning with two-dimensional detectors.

All the four approaches, *viz* peak-shift, FWHM, centroid-shift and segmental-shift show almost similar lattice strain (ε_h) distribution profiles at different applied strains (ε_b) in the samples (Fig. 5a, 5b, 5c, 5d). Smoother profiles are observed in the case of peak-shift approach, but the direction of maximum strain was observed varying in all cases. With the loading direction along bone axis (β = 90 degrees) (Fig. 2), maximum strain is observed close to the loading direction in the case of segmental-shift approach compared to peak-shift, FWHM and centroid-shift approaches (Fig. 9). The segmental-shift has negligible error (S.D. = 0.96) compared to peak-shift (S.D. = 6.44), FWHM (S.D. = 9.26) and centroid-shift (SD = 7.85). The negligible error in mean maximum strain along loading direction suggests reliable strain values along other azimuthal directions as well from the segmental-shift approach.

Although we used similar weighted average approximation for intensities at all radial positions from the array of raw pixel intensities, the measured crystal strain (ε_h) shows agreement with applied sample strain (ε_b) with higher R^2 values (99.49 %) in segmental-shift method compared to peak-shift method (R^2 = 98.44 %), FWHM method (R^2 = 95.24 %) and centroid-shift method (R^2 = 97.76 %) (Fig. 6). The mean of strain ratio ($\varepsilon_h/\varepsilon_b$) showed standard errors 0.066 for peal-shift, 0.117 for FWHM and 0.079 for centroid-shift, whereas segmental-shift has comparatively less standard error equal to 0.035 (Fig. 7). Comparing strains along loading direction (ε_h) with our

previous results (Fujisaki *et al*, 2006), we obtained almost similar standard error range in the case of imaging plate using segmental-shift method (S.D. = 112 for IP and 101 for scintillation counter) (Fig. 8). Furthermore, the strains calculated by weighted average yielded overall less error in the values. For peak-shift and FWHM, the standard errors are respectively 918 and 390 in the case of scintillation counter, whereas they are respectively 168.88 and 183.6 in the case of IP.

We also attempted to compare Poisson's ratio at different loading condition. Poisson's ratio obtained from applied tissue strain is nearly similar in all the loading cases with average value of 0.34 (Fig. 10a). Poisson's ratio calculated considering two orthogonal lattice strains (- $\varepsilon_h^0/\varepsilon_h^{90}$) showed almost identical mean values for 1000 and 2000 micro-strains of applied load in all the four approaches and unexpectedly lower values at 1500 micro-strains (Fig. 10b). Poisson's ratio at 500 micro-strains reflects higher range of deviation in all the four approaches; centroid-shift shows negligible value. The large range of errors is because of variation in the calculated values in different samples ranging from below zero to above one. Such anomalous behavior in Poisson's ratio obtained from lattice strains could be regarded to the anisotropic character of bone tissue and expansion contraction attribute of lattice planes with external loads. Since our calculation is based on the strains of a particular lattice plane *(211)*, it implies the need of improvement or discovery in the approach of obtaining Poisson's ratio for crystals rather than considering lattice strains.

While using different techniques for peak determination, the approaches are only valid so far the profiles represent distinct peaks. So far material with low crystallinity like the bone is considered, the diffracted intensity has diffused profile near the peak and may include information of several irregular lattice planes. In our point of view, the peak position even if determined from any functional fitting in such case may

represent of a single regular plane. We also believe that the broad and irregular diffraction profile from low crystalline material like bone tissues is difficult to be explained from mathematical function simply. On the other hand, consideration of centre of gravity of a profile has drawback that it is greatly affected by the selection of background. The situation will further worsen when the peak is broad and multiple profiles are very close (as in the case of bone). In this regard the authors' proposed technique (Fujisaki *et al*, 2006), which does not require any profile fitting routine or knowledge of peak/s but considers the integrated shift of profile segment, proves to be appropriate for bone tissues.

Although the intensity profile has a broader peak for low crystalline material like minerals of bone tissue, the analysis was performed with *(211)* plane in spite of its possibility to overlap with neighboring peaks, because the intensity throughout the Debye ring is uniformly distributed for this plane irrespective of preferred orientation of crystals. The approach in segmental-shift method is under the assumption that the diffraction profile consists of number of irregular peaks. The method does not require the ideal peak position, and does not consider the number of peaks associated (in case of overlapping profile) as well. The integrated shift of profile segment is considered for the necessary analysis. Hence, the technique is rather advantageous using complex planes, especially in the case of low crystalline materials like living bone tissue. This consideration will also be of advantageous when major structural information is necessary.

Placing a two-dimensional detector perpendicular to the direction of incident beams (or inclined to beam with corresponding correction) and assumption of two coordinate axes with pixels along vertical and horizontal direction is a basic practice in X-ray diffraction imaging procedures. But other considerations, like initial

calibration of images, beam centre from the whole image intensity distribution, width of incident beam, particular 2-theta position, etc also will have effect on the results, and which do not have any specific rule or process to follow but basically depends on choice of the investigator. Using X-ray intensity distribution profile in the two-dimensional detector though possesses various advantages if carried out properly, due consideration on precise tagging of pixels data needs to be focused more. The weighted average of intensity values used in this work could be one of the solutions for precise data extraction.

For laboratory X-ray system, we also performed extent of sensitivity in the deformation by different resolution scan of IP (100 μm and 50 μm), change in camera length and change in collimator diameter (1 mm and 0.5 mm). We observed significant relationship among them (detail not shown here). High resolution images and larger camera length resulted in less error in the values. But other factors associated with this, like intensity of X-rays, data scan and analysis duration, etc further needs to be considered.

Among very few literatures existing on lattice deformation measurements in bone tissue, most particularly make use of high energy X-rays for diffraction phenomena with the peak of profiles approximated with mathematical functions (Almer and Stock, 2007; Almer and Stock, 2005; Gupta *et al*, 2006, etc). In the current work, we have carried out experiment with weak X-rays and the outcomes presented do not consider any profile approximation function. This is considered a step forward towards our aim of devising a methodology and developing a useful technique that could be ultimately applied with living bone tissues in clinical practice. Our attempt in this work is to particularly advance the accuracy and precise for such application.

5. Concluding remarks

The current study gives a comparative analysis of widely accepted standard approaches - peak-shift, FWHM and centroid-shift - with segmental-shift approach and presents convincing results for accuracy, reliability and effectiveness of segmental-shift method compared to others in the application of two-dimensional detector. Our weighted average approach of integrating intensity values from digital pixel data with precise radius vector positioning is expected to give the outcomes more accurately than previously applied direct pixel value adaptation, especially in the case of larger pixel step area. This also draws the concentration of researchers involved in such application for more considerations on X-ray data extraction process and gives possibility of various approximations instead of direct pixel value adaptation for precise outcomes. The current work hence adds one more step to the difficult area of study of bone strain quantification with clinical relevance using weaker X-rays.

Acknowledgement

This work was supported by Grant-in-Aid for Scientific Research (B), MEXT (No. 16300143) and (A), MEXT (No. 19200035).

References

Almer, J.D., Stock, S.R., 2005. Internal strains and stresses measured in cortical bone via high-energy X-ray diffraction. Journal of Structural Biology 152, 14-27.

Almer, J.D., Stock, S.R., 2007. Micromechanical response of mineral and collagen phases in bone. Journal of Structural Biology 157, 365-370.

Borsato, K.S., Sasaki, N., 1997. Measurement of partition of stress between mineral and collagen phases in bone using X-ray diffraction techniques. Journal of Biomechanics 30, 955-957.

Cullity, B.D., Stock, S.R., 2001. Elements of X-ray Diffraction. Prentice-Hall, USA.

Currey, J.D., 1969. The mechanical consequences of variation in the mineral content of bone. Journal of Biomechanics 2, 1-11.

Fujisaki, K., Tadano, S., 2007. Relationship between bone tissue strain and lattice strain of HAp crystals in bovine cortical bone under tensile loading. Journal of Biomechanics 40, 1832-1838.

Fujisaki, K., Tadano, S., Sasaki, N., 2006. A method on strain measurement of HAp in cortical bone from diffusive profile of X-ray diffraction. Journal of Biomechanics 39, 579-586.

Giri, B., Tadano, S., Fujisaki, K., Todoh, M., 2007. Microstructure of bone around natural hole in bovine lumbar vertebra. Journal of Biomechanical Science and Engineering 2, 1-11.

Gupta, H.S., Messmer, P., Roschger, P., Bernstorff, S., Klaushofer, K., Fratzl, P., 2004. Synchrotron diffraction study of deformation mechanisms in mineralized tendon. Physical Review Letters 93, 158101 (1-4).

Gupta, H.S., Seto, J., Wagermaier, W., Zaslansky, P., Boesecke, P., Fratzl, P., 2006. Cooperative deformation of mineral and collagen in bone at the nanoscale. PNAS 103, 17741-17746.

Gupta, H.S., Wagermaier, W., Zickler, G.A., Aroush, D.R.B., Funari, S.S., Roschger, P., Wagner, H.D., Fratzl, P., 2005. Nanoscale deformation mechanisms in bone. Nano Letters 5, 2108-2111.

Hammersley, A.P., Svensson, S.O., Hanfland, M., Fitch, A.N., Häusermann, D., 1996. Two-dimensional detector software: From real detector to idealized image or two-theta scan. High Pressure Research 14, 235-248.

He, B.B., Preckwinkel, U., Smith, K.L., 1999. Fundamentals of two-dimensional X-ray diffraction. Advances in X-ray Analysis 43, 273-280.

Noyan, I.C., Cohen, J.B., 1987. Residual Stress Measurement by Diffraction and Interpretation. Springer-Verlag, New York, p.164-181.

Rodriguez-Navarro, A.B., 2006. XRD2DScan: new software for polycrystalline materials characterization using two-dimensional X-ray diffraction. Journal of Applied Crystallography 39, 905-909.

Tadano, S., Okoshi, T., 2006. Residual stress in bone structure and tissue of rabbit's tibiofibula. Bio-Medical Materials and Engineering 16, 11-21.

Figures Legend

Figure 1 Diffraction profile shift measurement approaches - (a) widely applied peak-shift and shift of FWHM, (b) Segmental-shift approach proposed by Fujisaki *et al* (2006). Centroid-shift, preferable for full profile consideration, is calculated by $<2\theta_c> = \int I(2\theta).2\theta.d(2\theta) / \int I(2\theta).d(2\theta)$.

Figure 2 Cortical strip from bovine femur (40×6×0.8 mm) attached to tensile loading device. Strain gage was glued to record applied strain in the specimen.

Figure 3 (a) Schematic diagram of X-ray diffraction phenomena using imaging plate (IP) system. (b) Experimental set up with IP system. Diffracted rays are detected by the IP. Image with series of Debye rings, each ring representing diffractions from different lattice planes will be observed on IP readout (Fig. 4). Notations are as used in the article.

Figure 4 A two-dimensional X-ray diffraction pattern sample obtained in 1140×1140 pixels area. Intensity in *(211)* is considered for strain measurements. Intensity patterns were converted to Cartesian distribution (2θ along x-axis, intensity values along y-axis) for each degree of azimuthal angle (β).

Figure 5 Distribution of strain along azimuthal directions derived from (a) peak-shift, (b) FWHM, (c) centroid-shift and (d) segmental-shift approaches. Zero-strain line separates tensile and compressive regions.

Figure 6 Correlation between applied tissue strain (ε_b) and measured lattice strain (ε_h). Segmental-shift approach gives closer relationship having lower R^2 value.

Figure 7 Ratio of measured lattice strain (ε_h) to applied sample strain (ε_b) (mean±S.D., n = 5) – (i) Peak-shift = 0.53±0.06, (ii) FWHM = 0.46±0.11, (iii) Centroid-shift (CS) = 0.49±0.08 (iv) Segmental-shift (SS) = 0.62±0.03. SS gave lower standard error.

Figure 8 Comparison of lattice strain along loading direction (ε_h) with the previous results using scintillation counter (SC) (Fujisaki *et al*, 2006) at 1000 micro applied strain. Almost similar standard error range in the case of imaging plate was observed by segmental-shift (SS). Lower standard errors were also obtained in case of imaging plate for all the three approaches (n = 5). Errors using IP - 18.5 (peak-shift), 12.9 (FWHM) and 9.6 (SS).

Figure 9 Maximum strain direction (mean±S.D., n = 5). Maximum strain is along 89.75 degrees with negligible error in case of segmental-shift (SS) approach (S.D. for peak-shift = 6.44, for FWHM = 9.26, for centroid-shift (CS) = 7.85, for segmental-shift (SS) = 0.96) (loading direction, β = 90 degrees).

Figure 10 (a) Poisson's ratio at different applied strains (ν = - lateral strain/longitudinal strain). The average value calculated from strain gage glued to the specimen is 0.34. (b) Poisson's ratio calculated from lattice strains (- $\varepsilon_h^0/\varepsilon_h^{90}$) in peak-shift, FWHM, centroid-shift (CS) and segmental-shift (SS) approaches. Anomalous behavior is observed.

Figure 1

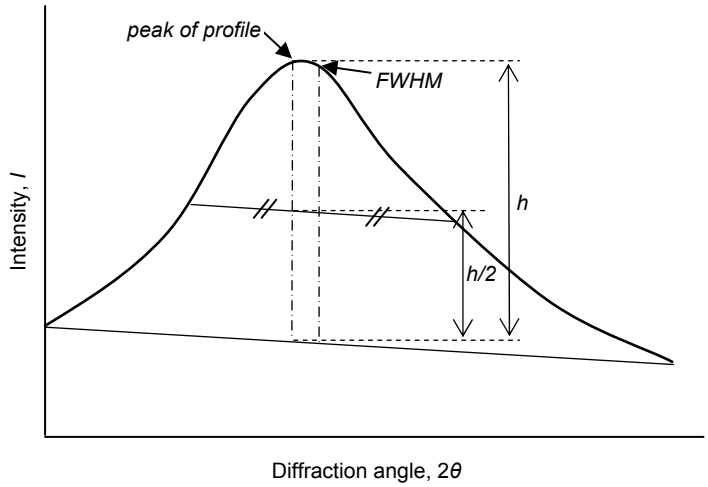
peak of profile
FWHM
h
h/2
Intensity, I
Diffraction angle, 2θ

(a)

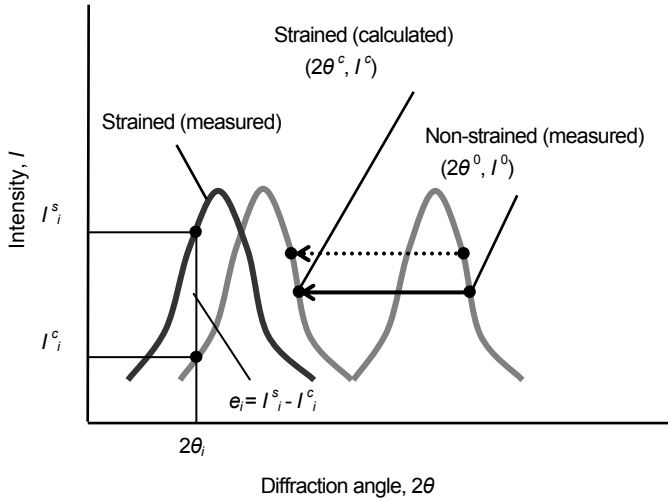
Strained (calculated)
(2θ c, I c)
Strained (measured)
Non-strained (measured)
(2θ 0, I 0)
Intensity, I
I s i
I c i
e i = I s i - I c i
2θ i
Diffraction angle, 2θ

(b)

Figure 2

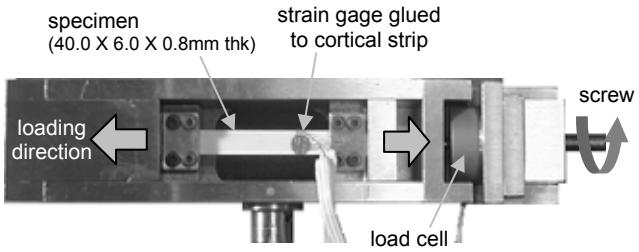
specimen
(40.0 X 6.0 X 0.8mm thk)
strain gage glued
to cortical strip
screw
loading
direction
load cell

Figure 3

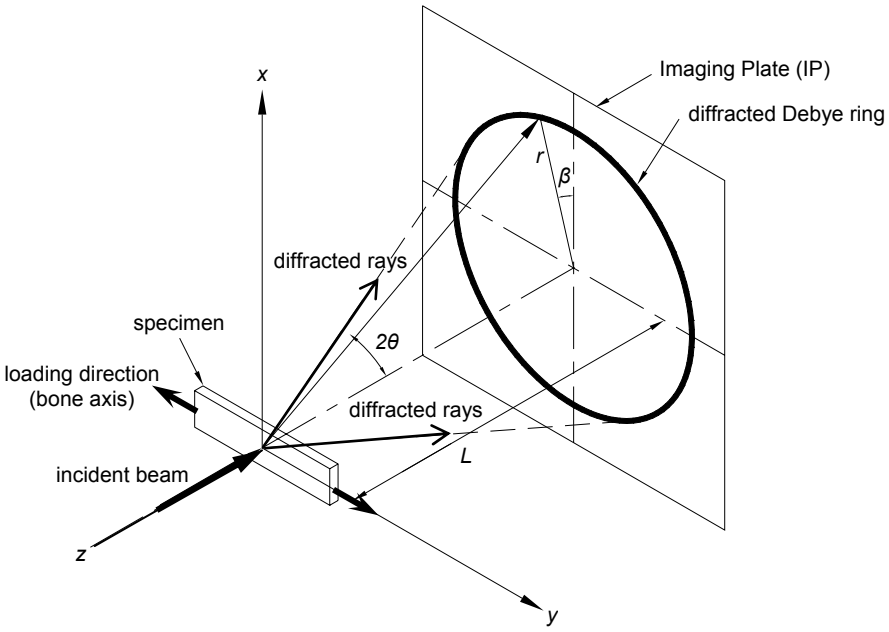
x
Imaging Plate (IP)
diffracted Debye ring
r
β
diffracted rays
specimen
2θ
loading direction
(bone axis)
diffracted rays
L
incident beam
z
y

(a)

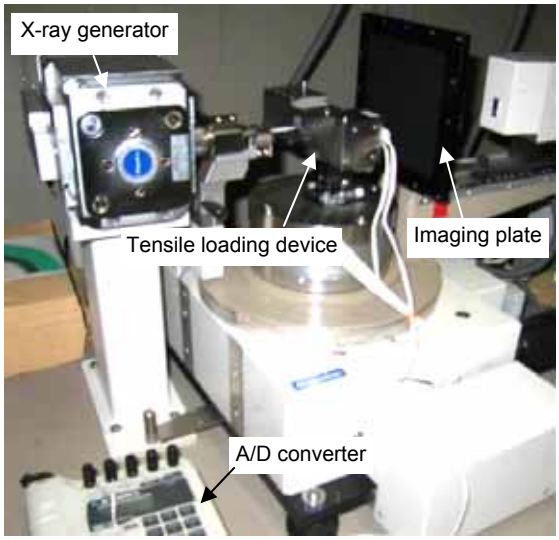
X-ray generator
Tensile loading device
Imaging plate
A/D converter

(b)

Figure 4

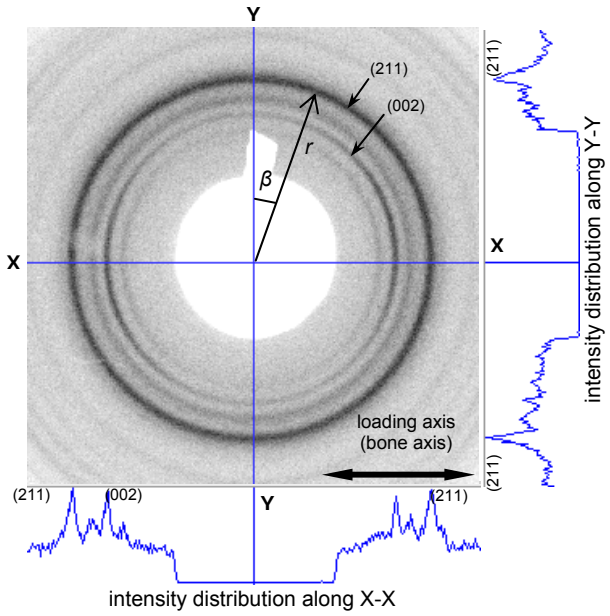
Y
(211)
(002)
r
β
X
X
(211)
intensity distribution along Y-Y
loading axis
(bone axis)
(211)
(211)
(002)
(211)
Y
intensity distribution along X-X

Figure 5

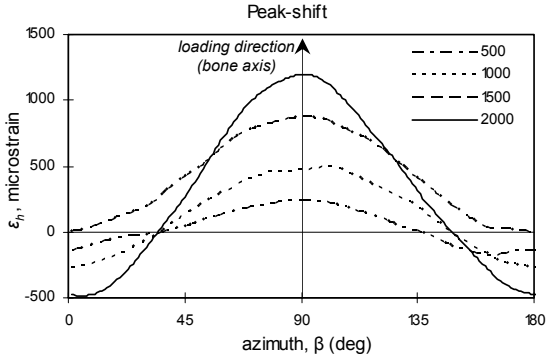
Peak-shift
loading direction
(bone axis)
500
1000
1500
2000
ε_h, microstrain
1500
1000
500
0
-500
0
45
90
135
180
azimuth, β (deg)

(a)

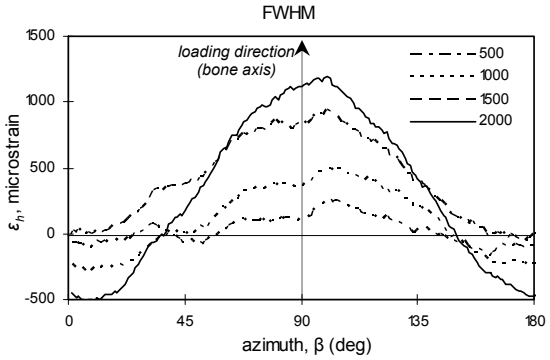
FWHM
loading direction
(bone axis)
500
1000
1500
2000
ε_h, microstrain
1500
1000
500
0
-500
0
45
90
135
180
azimuth, β (deg)

(b)

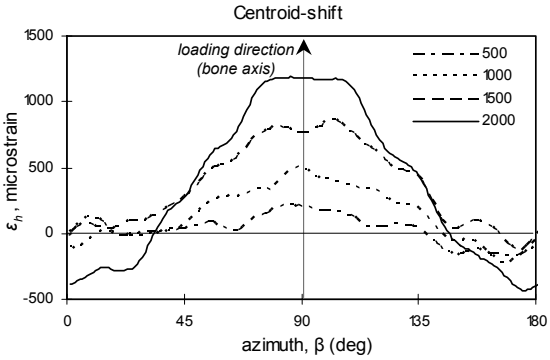
Centroid-shift
loading direction
(bone axis)
500
1000
1500
2000
ε_h, microstrain
1500
1000
500
0
-500
0
45
90
135
180
azimuth, β (deg)

(c)

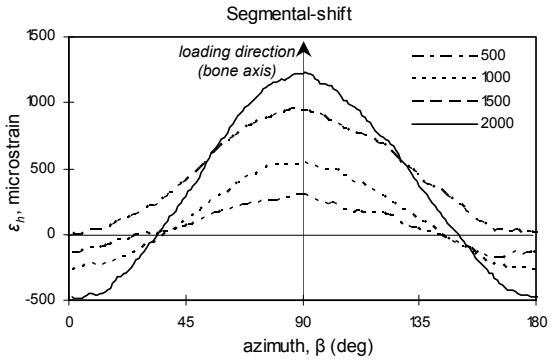
Segmental-shift
loading direction
(bone axis)
500
1000
1500
2000
1500
1000
500
0
-500
ε_n, microstrain
0
45
90
135
180
azimuth, β (deg)

(d)

Figure 6

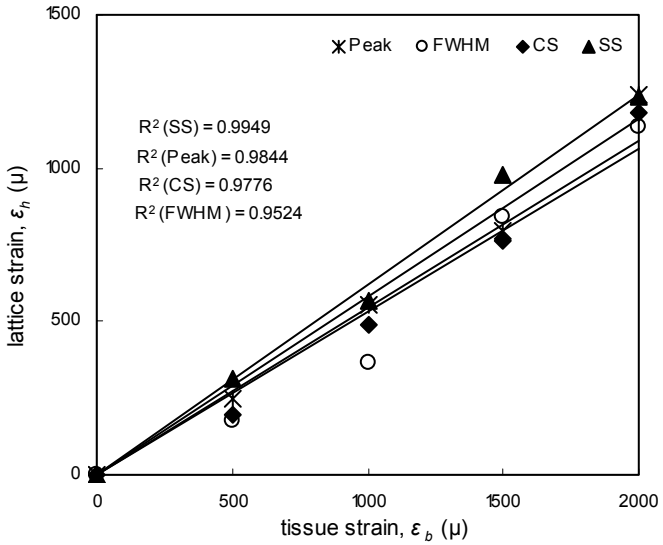
Peak
FWHM
CS
SS
R² (SS) = 0.9949
R² (Peak) = 0.9844
R² (CS) = 0.9776
R² (FWHM) = 0.9524
lattice strain, ε_h (μ)
tissue strain, ε_b (μ)
0
500
1000
1500
2000

Figure 7

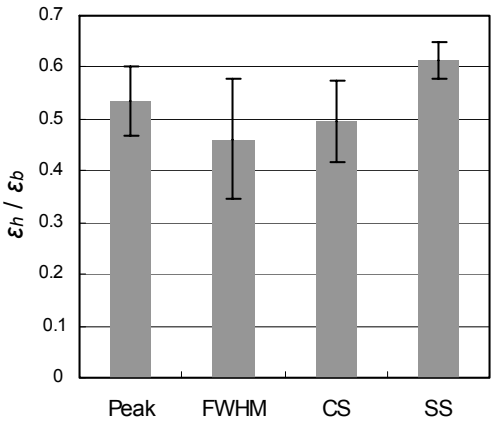

Figure 8

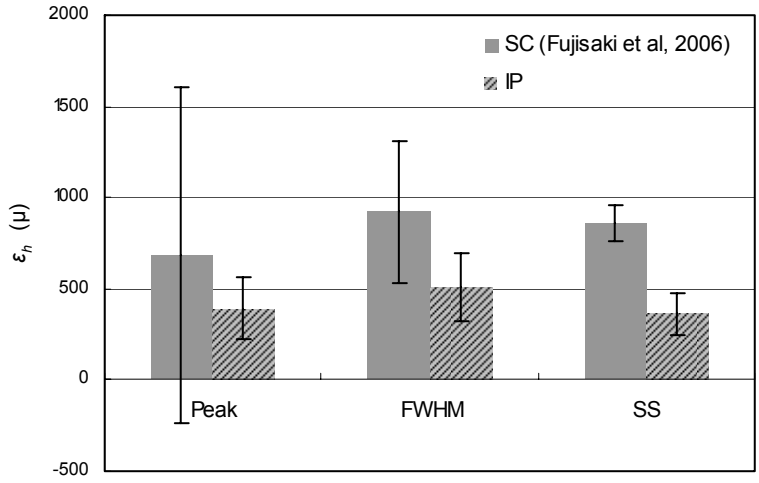
2000
1500
1000
500
0
-500
ε_h (μ)
SC (Fujisaki et al, 2006)
IP
Peak
FWHM
SS

Figure 9

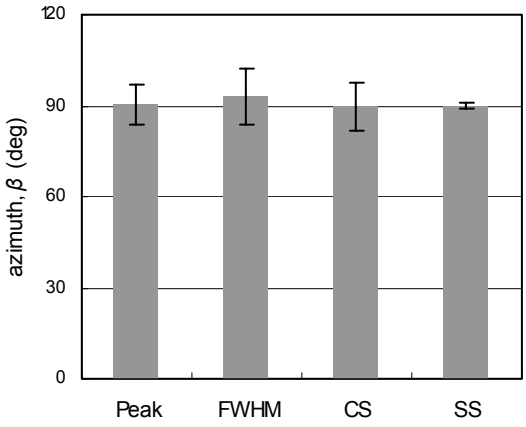

Figure 10

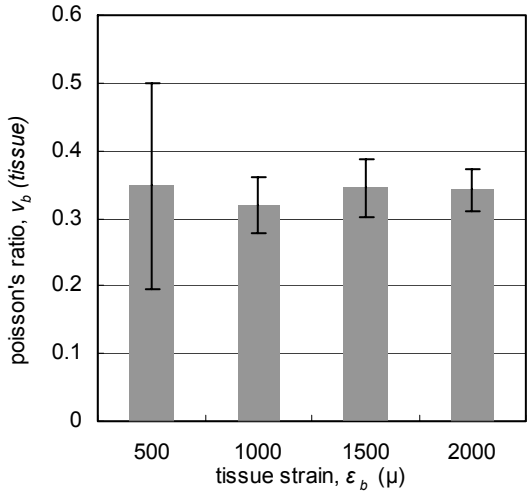
0.6
0.5
0.4
0.3
0.2
0.1
0
poisson's ratio, v_b (tissue)
500
1000
1500
2000
tissue strain, ε_b (μ)

(a)

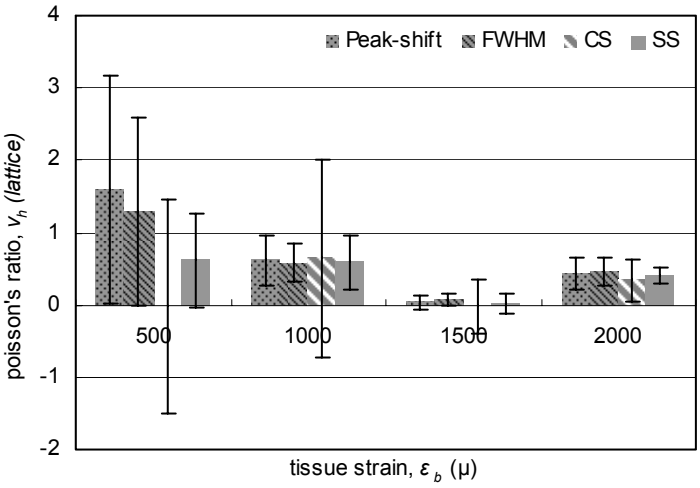
Peak-shift
FWHM
CS
SS
4
3
2
1
0
-1
-2
poisson's ratio, v_h (lattice)
500
1000
1500
2000
tissue strain, ε_b (μ)

(b)